Monitor the Processes of Ice Film Disappearance under a Stimulant Convection Condition and Absorption Ethanol Vapor to Ice by a Quartz Crystal Microbalance

Lei Yu[1], Xiaolong Ma[2], Ting Wu[2], Yangyang Ma[2], Dazhong Shen, Qi Kang[2,]*

[1]Department of Chemical Engineering and Environment, Weifang University of Science and Technology, Weifang 262700, P. R. China.
[2]College of Chemistry, Chemical Engineering and Materials Science, Collaborative Innovation Center of Functionalized Probes for Chemical Imaging in Universities of Shandong, Key Laboratory of Molecular and Nano Probes, Ministry of Education, Shandong Provincial Key Laboratory of Clean Production of Fine Chemicals, Shandong Normal University, Jinan 250014, P. R. China.
[*]E-mail: qikang@sdu.edu.cn

In this work, the processes of ice film disappearance under a stimulant convection conditions and absorption to ethanol vapor to ice film were monitored by a quartz crystal microbalance (QCM) technique. The influence of the thickness of ice film on the response of the QCM was investigated by an impedance analysis method. It is shown that part of freshly prepared amorphous ice film on QCM is disappeared gradually during a stimulant convection process at -18 °C. We report a mulriple resonance phenomenon in QCM with unsymmetrical mass loading. The shape of the conductance-frequency spectrum of QCM depends on the thickness and distribution of the ice film deposited. After adsorption of ethanol vapor, the rigidity of the ice film is decreased gradually. With a large amount of ethanol adsorbed, the ice film is dissolved and evaporated completely. The QCM is a useful tool to monitor the mass and rigidity change of ice film.

1. INTRODUCTION

Studies with the quartz crystal microbalance (QCM) sensor became popular after the pioneering work of Sauerbrey [1], which demonstrated proportionality between a mass change (Δ*m*)

on a quartz oscillator's electrode(s) and the associated frequency shift (ΔF), i.e, the so-called Sauerbrey equation in Eq.(1).

$$\Delta f = -2.26 \times 10^{-6} f_0^2 \frac{\Delta m}{A} \qquad (1)$$

where f_0 and A are the fundamental frequency and the electrode area of the QCM, respectively.

It has been successfully demonstrated the applications of QCM in gaseous sensors [2-4], electrochemistry [5-8], biosensors [9-14] and processes investigation [15,16]. In liquid phase measurements, the QCM is not a simple mass sensor, but provides valuable information about reactions and conditions at the liquid/solid interface [17, 18].

Ice is one of the most prevalent condensed phases present in the Earth's atmosphere. The physics and chemistry of ice surfaces has attracted considerable research interest in such diverse areas of science as environmental, interstellar, and biological chemistry [19-25]. Snow or ice represents an important environment in the atmosphere and on the earth's surface due to the fact that they play an important role in the storage and reactions of environmentally relevant trace gases [26]. A study of molecular adsorption on ice surface is important from an environmental chemistry point of view. Various methods, such as FTIR [27-30], X-ray photoelectron spectroscopy [29], ellipsometry [30], molecular dynamics simulation [31-33], ice chromatographic [34], Raman microscopy [35], coated-wall flow-tube [36], were employed to study the adsorption of gas molecules to ice. In most of the works related to the adsorption of gas molecules onto ice interface [37-43], the experimental conditions of very low temperature and pressure, which are similar to those in the troposphere of the Earth, were used. Some applications of QCM in the mass transfer at ice interface were reported. For example, Mason and Dash measured the mass transfer between two ice films in the processes of ice-ice collisions under a simulant thunderstorm electrification [44]. In the works of Delval and Rossi [45,46], the kinetics of condensation and evaporation of H_2O from pure ice in the range 173–223 K and the influence of monolayer amounts of HNO_3 on the evaporation rate of H_2O over ice in the range 179–208 K were studied under the pressure condition of vacuum. The sputter yield of ice molecules at the ice/vacuum interface in a secondary ion mass spectrometry was measured [47,48].

The motive of this work was to characterize adsorption of ice film at atmospheric pressure by the QCM technique. When a thin water film was froze on the surface of the QCM, part of the ice film was disappeared under a stimulant convection conditions. If the ice film was not uniform and thick enough, however, the normal symmetrical resonant peak of the QCM was split to a group of resonant peaks with much weaker intensity in a much broad span of frequency. During a stimulant convection process, the resonant peaks moved to higher frequency with increasing intensity. An equivalent circuit model with the parallel combination of resonators was used to estimate the resonant parameters of the resonant peaks. The averaged resonant frequency of the peaks with the square of peak intensity as the weighting factor was employed to estimate the averaged mass of the ice film. In addition, the dissolution process of a thin ice film induced by the absorption of ethanol vapor was monitored. The responses of the QCM, in the stages of adsorption and dissolution of the ice film, shrinkage and volatilization of the liquid film, were investigated.

2. EXPERIMENTAL

2.1. Setup for investigation of the stability of ice film

A schematic representation of the experimental setup for investigation the stability of ice film is presented in Fig.1A**.** The setup was mounted in a refrigerator (BCD-215KA, Hair, China). AT-cut 5 MHz piezoelectric quartz crystals with 14 mm wafer diameter (Model JA5, Beijing Chenjing Electronics Co., Ltd., China) were used. Two silver electrodes (key-hole configuration, geometric area = 0.407 cm^2) were deposited on both sides of the quartz wafer. To obtain a homogeneous ice film on the surface of the silver electrodes, QCM was immersed in 5 mM dopamine solution for 4 h to form a hydrophilic polydopamine layer. The QCM was mounted horizontally in the freezing room in a refrigerator. The temperature in the area near the ice film was recorded by a digital thermometer. The electrodes of QCM were connected to a precision impedance analyzer (Agilent 4294A) by coaxial-cable. A user program written in Visual Basic 6.0 was used to acquire and process the impedance data. To obtain the picture of the ice film, a digital video was put about 2 cm above the quartz crystal. And an LED light was employed to illumine the ice film. A plastic pipe with inner diameter of 5 mm was employed to deliver humid air flow for ice film deposition. The thickness of ice film was controlled by the interval of blowing wet air flow. The shifts in frequency and motional resistance were recorded to estimate the stability and rigidity of ice film.
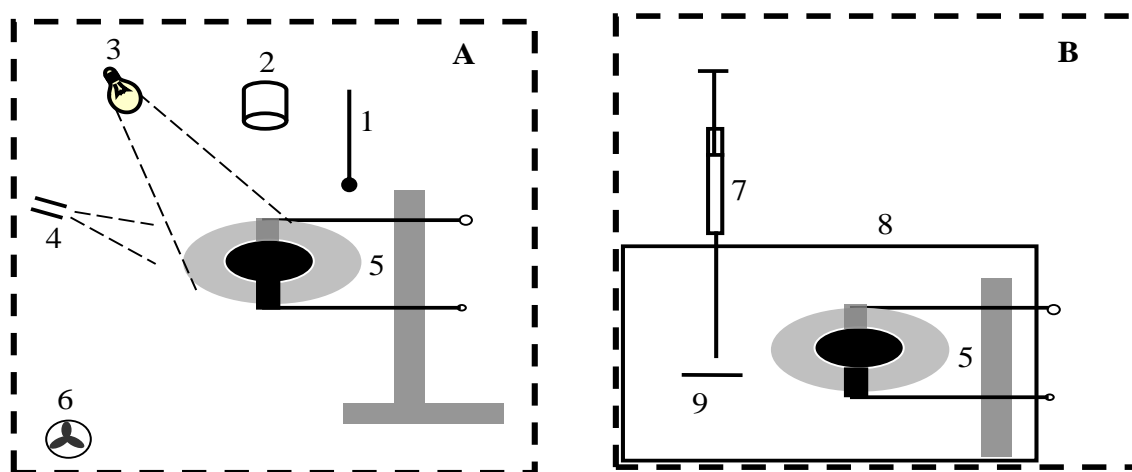

Figure 1. Schematic drawing of experimental setup employed for the ice film disappearance (A) and adsorption measurements (B) (not to scale). (1) digital thermometer; (2) digital video; (3) LED light; (4) humid air flow: (5) QCM with ice film； (6) mini fan; (7) microsyringe with ethanol ;（8）: adsorption box with outside ice wall; (9) filter paper .

In case of a relative thick ice film, a water film was spread on the upside surface of QCM at 4 °C by a soft cotton brush. Immediately, the QCM and its holder were put into the freezing room in a refrigerator. In the situation of resonant peak cleavage, the resonant frequency and motional resistance of the peaks were estimated by an iterative algorithm discussed in Section 3.3.To improve the

resolvability of the impedance data, the conductance (*G*) –frequency spectrum was measured in several successive scans if needed.

2.2 Monitor the adsorption of the vapor of ethanol on ice film by QCM

Prior to the fabrication of ice film, the QCM was frozen in an adsorption box (120 mL) with outside ice wall (Fig.1B) at -18 °C for 20 min. Then the cold QCM was in contact with the humid air at room temperature to obtain a homogeneous thin water film. Immediately, the QCM was froze again in the box for 4 h to form firm ice film on the surface of QCM. Whereafter, a given volume of precooled ethanol was injected in the adsorption box by a microsyringe. The adsorption process of ethanol vapor on the ice film was monitored by QCM in an impedance analysis method. The shifts in frequency and motional resistance were recorded to estimate the thickness of ice film.

3. RESULTS AND DISCUSSION

3.1 Influence of the thickness of ice film on its disappearance behavior

In the attempt to investigate the stability and adsorption behavior of ice film, we deposited an ice film on the surface of QCM by a freezing method illustrated in Fig.1A. Under our experimental conditions, part of tiny water drops in the humid air flow were expected to condensate firstly on the surface of QCM. Then the water layer was froze further to an ice film. With increasing blowing time, more water was condensated. As shown in Fig.2A, the resonant frequency of the QCM was decreased immediately upon contact with the humid air flow. With a blowing time of 3,6 and 9 s, the resonant frequency of the QCM was decreased by 1.66, 5.43 and 15.3 kHz in 30, 44 and 69 s, respectively. The decrease in the frequency was due to the deposition of ice film on the surface of QCM. According to the Sauerbrey equation, the corresponding thickness of the ice film is 0.32, 1.05 and 2.95 μm, respectively. However, the increase in frequency was observed in the late stage of freezing process, revealing that part of the ice film was disappeared gradually, especially in the case of thin film (curve a). When the frequency reached a stable level again, the residual ice film is 4%, 27% and 59% of the initial one deposition with the blowing time of 3, 6, and 9 s, respectively.

It should be noted that the motional resistance of the QCM is an indicator for the rigidity of the film deposited. The more rigid of the film, the less of the motional resistance. For example, the motional resistance of the blank QCM is ca. 9 Ω. When one side the QCM was in contact with a water layer at 25 °C, the motional resistance was increased to 389 Ω. The reason is that a non-rigid liquid film causes additional energy loss in QCM resonance, resulting in the increase on the motional resistance. Under our experimental conditions, the changes in motional resistance of the QCM were measured and shown in Fig.2B. After in contact with the humid air flow, the motional resistance of the QCM was increased rapidly to a maximum then reduced to the previous level in the late stage of freezing process. The increase in motional resistance was ascribed to the appearance of water layer on

the surface of the QCM. As the maximum of R_q is less than 380 Ω, we can conclude that the initial deposition layer is the composite of water and ice.
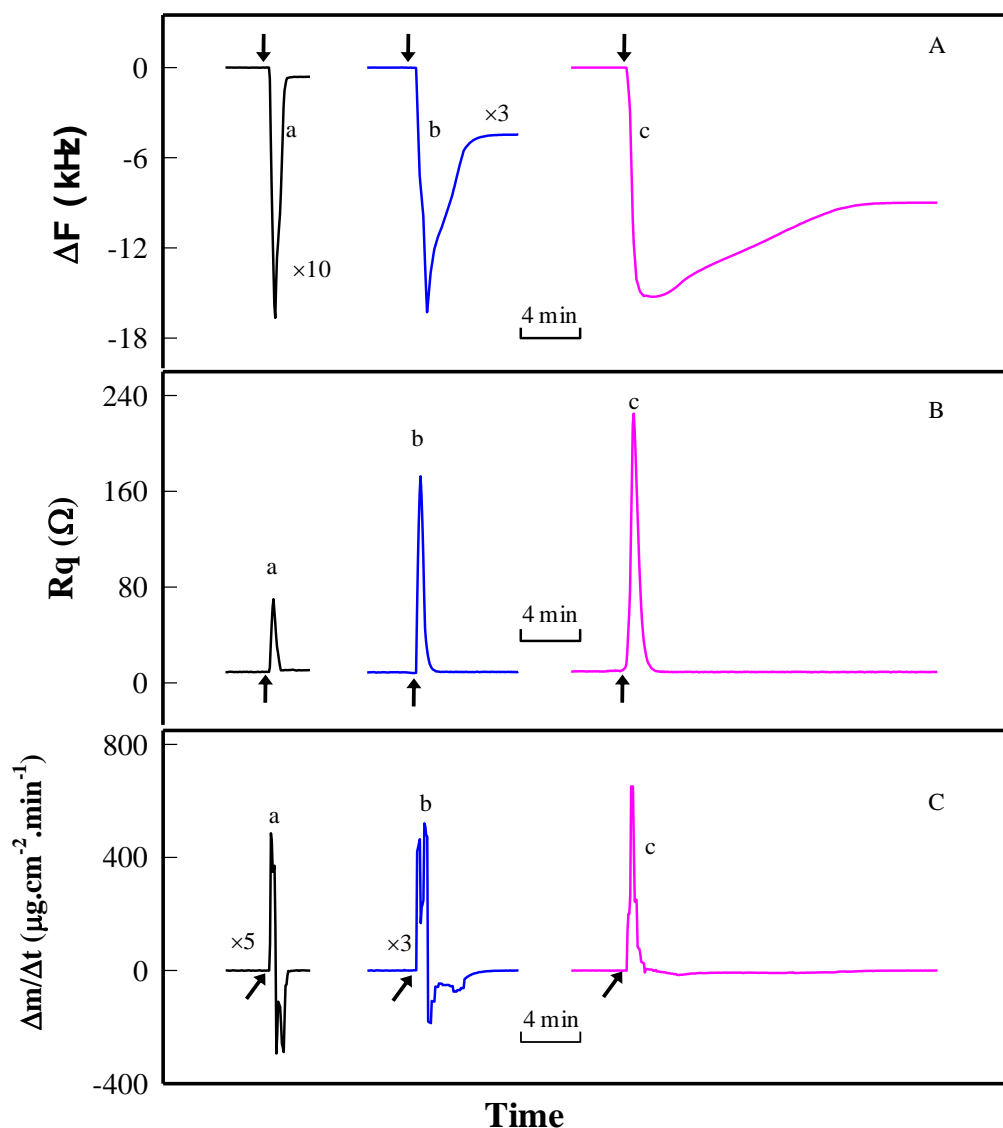

Figure 2. Changes of the resonant frequency (A) , motional resistance (B) and mass deposition rate (C) during the freezing process. Blowing time for humid air flow: (a): 3 s, (b): 6 s; (c): 9 s.

With increasing blowing time, the area and thickness of the water/ice composite were enlarged. And the duration of the water in the composite is 41, 59 and 78 s in curves a,b,and c, respectively.

In the measurement of a QCM sensor, an ultrathin, homogeneous and rigid film is needed in the calculation of mass change by the Sauerbrey equation. In the initial deposition stage, the water/ice composite is non-rigid, the mass and viscous models of the QCM were measured.

When the QCM was in contact with a liquid phase, the change in frequency due to viscous response was derived by Kanazawa and Gordon [49]

$$\Delta F_{viscous} = -f_0^{3/2} [\frac{\eta \rho}{\pi \mu_q \rho_q}]^{1/2} \qquad (2)$$

Where η and ρ are the viscosity and density of the liquid, respectively, and μ_q and ρ_q are the elastic modulus and the density of the quartz, respectively.

Muramatsu et al. [50] showed that the change in motional resistance, ΔR_q, of QCM in contact with a liquid phase can be expressed by

$$\Delta R_q = \frac{A(2\pi f_0 \eta \rho)^{1/2}}{K^2} \qquad (3)$$

where η and ρ are the viscosity and density of the liquid, respectively, K^2 is the electromechanical coupling factor.

To estimate the mass of the ice film, the frequency shift from the viscous response of water layer was corrected by using the correlation between ΔR_q and $\Delta F_{viscous}$ in Eq.(2) and (3). Under our experimental conditions, $\Delta F_{viscous} = -2.157 \Delta R_q$ was obtained in a group of glycerol aqueous solutions in concentration range of 0 to 50%. And the corrected frequency (ΔF - $\Delta F_{viscous}$) was used to calculate the mass change on the surface of QCM. As can be seen in Fig.2C, the amount of ice deposited was increased with increasing rate, which is due to the transform of non-rigid water layer to rigid ice film in the initial freezing stage.

It is well known that the melting point of ice is 0 °C. But the freshly deposited ice film was lost at a considerable rate even at the temperature of -18 °C. The loss of the ice film may be due to the loose structure of the initial ice film. It is possible that an amorphous ice film (like hoarfrost) was formed on the surface of QCM. Because the interaction between the ice microcrystals in the ice film is relatively weak, part of them were shed by the airflow in the freezing room. The airflow may be caused by the blowing air flow or the temperature difference near the QCM in the condensation and freezing stages. As the freezing time prolonged, the loose hoarfrost film was transformed gradually to compact ice film, the intensity of airflow was weakened. Hence, the stability of the resultant ice film was enhanced. Another possible reason is due to the sublimation of ice film. It was reported the ice layers of 2-30 nm deposited on the Pt(111) and graphite (0001) surfaces is sublimated even at 145-150 K under high vacuum and the sublimation rate depends strongly on the underlying substrate [51]. The kinetics of condensation and evaporation of H_2O from pure ice in the range 173–223 K was investigated by QCM [45].

3.2 Responses of QCM in the situation of heavy and unsymmetrical mass loading

To observe how the ice film was disappeared from the surface of the QCM, a digital video was mount above the quartz crystal (Fig.1A). But the transparence of ice makes it difficult to view a thin ice film. For the consideration of view ice film, a thicker ice film was prepared by spreading water film on the electrode surface of QCM.

As shown in Fig.3, a symmetrical resonant peak was obtained in the QCM in contact with water film (curve 1). After the QCM and holder were put into freezing room for 105 s, the resonant peak was damped to a chunky one with a shoulder peak (curve 2). The peak width at half height was

increased to 393 kHz, which is about 22 times of that in curve 1. The maximum conductance and corresponding frequency were reduced to 0.097 mS and 4.9103 MHz, respectively.The damping of the resonant peak is due mainly to the increase in the viscosity of the super-cooling water layer.
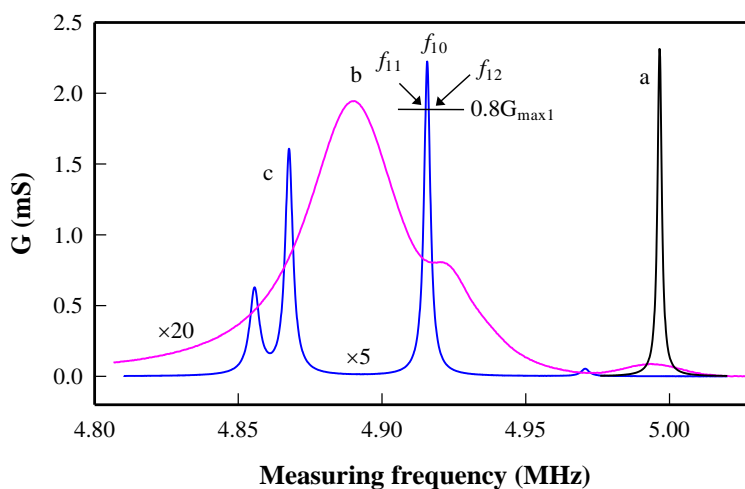

Figure 3. Typical conductance-frequency spectra of the QCM during the freezing process of spread thin water film. (a) initial water film in freezing room (*t*=0); (b) mixture of water and ice films (*t*=105 s) ; (c) initial ice film (*t*=122 s)

As the freezing time was prolonged, the temperature of QCM was expected to decline further until to reach itssurrounding temperature. Then the super-cooling water layer was changed to an ice film rapidly. As a result, the rigidity of the loading film was increased abruptly and the interaction between ice film and the surface of QCM was much enhanced. Interestingly, the previous chunky resonant peak was replaced suddenly by a group of small symmetrical resonant peaks in the conductance-frequency curve (curve 3). Due to the limit of scan rate of the impedance analyzer, the detailed responses of QCM in intermediate stage between two scans (from a chunky resonant peak to mulriple resonant peaks) were missed. The mechanism of mulriple resonance of the QCM a relatively thick ice film is not clear. We assume it may be related to the overloading and asymmetrical distribution of ice film on the surface of QCM.

However, if a thicker water layer (ca. 0.7 mm) was spread, the response of the QCM is much different.Upon freezing, the resonant frequency and peak height are reduced gradually. The appearance of ice crystal in the liquid layer is indicated by the abrupt decrease in the resonance. With ice film formed, the conductance-frequency curve is unsymmetrical and the frequency at G_{max} is even 17.3 kHz higher than the frequency of the blank QCM (data are not shown). Similar experimental phenomenon was reported and explained by the presence of a "like-liquid-layer" in interface of QCM/ice film in Refs. [52,53], in which an ice layer with the thickness of ca. 5-10 mm was prepared on the surface of the electrode. The response of QCM to a liquid-like layer at the ice/metal interface was investigated and the thickness of the liquid-like layer was measured directly using QCM [53]. Under our

experimental conditions, the resonance of QCM was decreased further until became undetectable after a freezing time of 10 min (data are not shown).

To test the influence of airflow on the stability of the prepared ice film, a mini fan was mounted in corner of the freezing room to generate a continuous cold breeze. Fig. 4 shows a group of typical responses of QCM and the corresponding picture of the ice film during the simulant convection process. Before the convection operation, the electrode surface was covered fully by an ice film and five resonant peaks and three shoulder peaks were observed in the frequency region from 4.5~5.1 MHz (Fig.4A). Because the difficulty to prepare two identical ice films by the spread method, the conductance-frequency spectrum in Fig.4A is different to that of curve 3 in Fig.3.
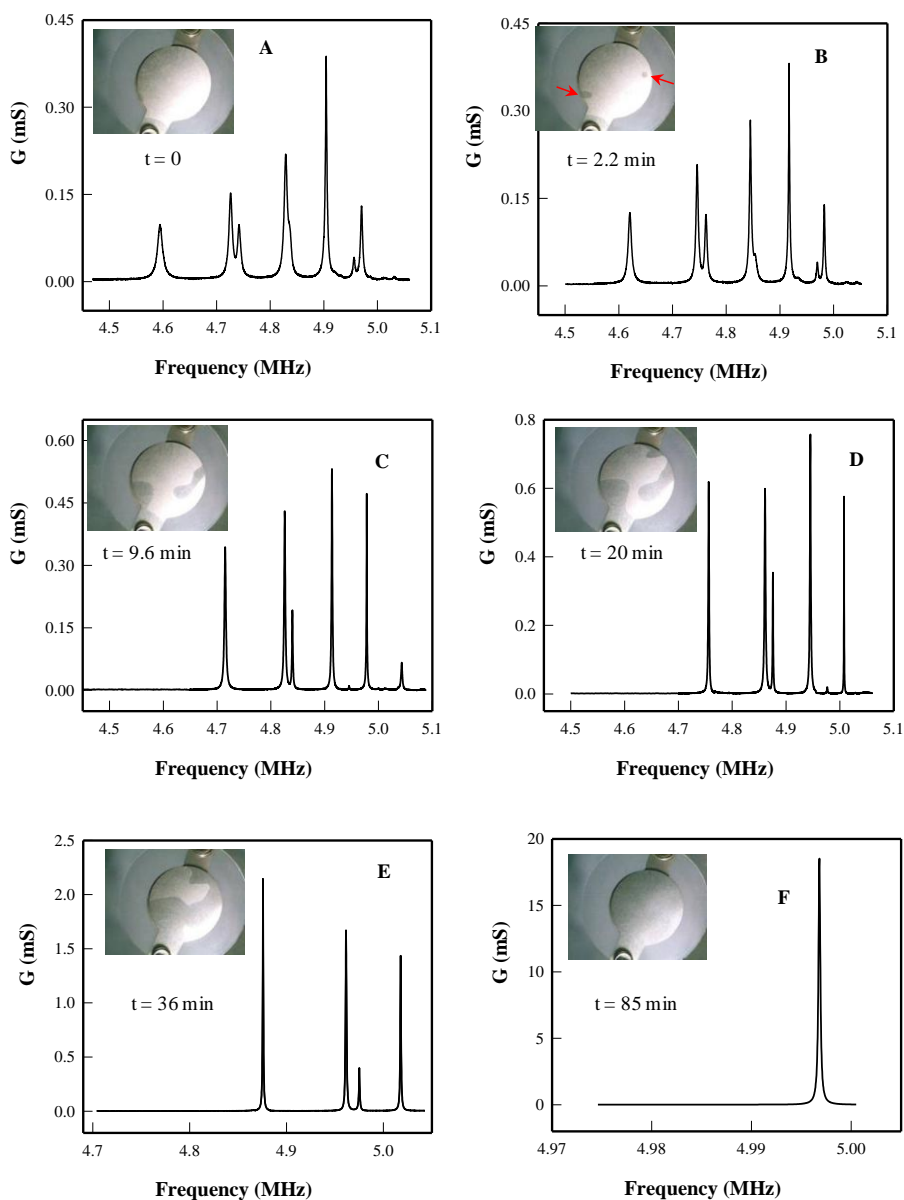

Figure 4. Representative conductance-frequency curve of the QCM and corresponding picture during a simulant convection process in freezing room (-18°C).

In the presence of the continuous cold airflow in the freezing room, two small defects occurred in the initial ice hoarfrost film (arrows in Fig.4B). The defects were ascribed to the disappearance of the ice film by the airflow. As the breezing time increased, the area of the defects in the ice film was enlarged gradually and the resonant peaks were shifted to higher frequency with increasing intensity (Fig.4C). In Fig.4D, 39.5 % of the ice film was disappeared, the strongest peak among five resonant peaks was shifted to 4.945 MHz with a height of 759 μS. After a convection time of 36 min, 62.8% of the ice film was shed, and four resonant peaks were detected (Fig.4E). The significant increase in the intensity of the resonant peaks may be due the disappearance of the ice film in the center part of the electrode. After a convection time of 85 min, the ice film was invisible in the picture in Fig.4F, only one peak with the height of 18.5 mS was observed. On the other hand, the resonant frequency is 3358 Hz lower than that of the initial blank QCM, indicating that a tiny ice layer is remained on the surface of QCM. This thin ice layer was not detected by the video because its transparency.

3.3 The information analysis of QCM in the condition of peak cleavage

When a thick and uneven ice film was deposited on the surface of QCM, as discussed above, the normal single resonant peak of QCM was split to a group of small peaks. During the disappearance process of the ice film, the frequency and intensity of the peaks were increased significantly. Hence, it is possible to monitor the mass change of the ice film by QCM. However, such film does not meet the prerequisite in the Sauerbery equation. To explore such possibility, the resonant frequencies of the small peaks were estimated from the conductance-frequency spectrum based on an equivalent circuit model in Fig.5A. In this model, a group of resonators in a parallel combination was employed to describe the resonance of QCM under the non-ideal conditions. The resonators denoted by 1,2 …n with decreasing intensity. These resonators were assumed to distribute in different areas on the quartz crystal disc.
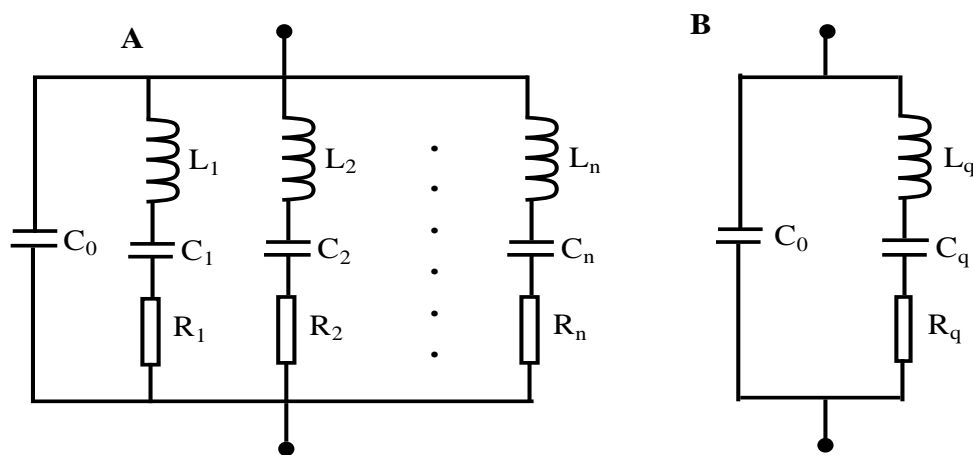

Figure 5. Equivalent circuit models of quartz resonator with mulriple resonance (A) and classical fitting model of QCM in impedance analyzer (B). C_0 R_q, L_q and C_q are the static capacitance, motional resistance, motional inductance and motional capacitance of the QCM with single resonant peak , respectively. R_i, L_i and C_i ($i=1, 2, …, n$) are the motional resistance, motional inductance and motional capacitance of the ith resonator, respectively.

The resonance of the quartz crystal disc is related to the interaction of all the resonators, which are dependent and influenced each other. Obviously, if a rigid, uniform and ultra-thin mass loading film is deposited on the surface of QCM, the equivalent circuit parameters of all the resonators are the same. The equivalent circuit model in Fig.5A is returned to that in Fig.5B, which is the normal equivalent circuit model for QCM.

According to the model in Fig.5A, the conductance of the primary resonant peak ($L_1C_1R_1$ branch), G_1, is expressed as

$$G_1 = \frac{R_1}{R_1^2 + X_1^2} \qquad (4)$$

where, $X_1 = \omega L_1 - \dfrac{1}{\omega C_1}$, $\omega = 2\pi f$, f is measuring frequency, R_1、L_1、C_1 are motional resistance, motional inductance and motional capacitance of primary resonator, respectively.

As can be seen in Eq.(4), G_1 has the maximum of $G_{max1}=1/R_1$ at the point of $X_1 = 0$. Accordingly, the resonant frequency of the primary resonator (f_{10}) is expressed by

$$f_{10} = \frac{1}{2\pi\sqrt{L_1C_1}} \qquad (5)$$

To estimate the equivalent circuit parameters of the resonator, two frequencies corresponding to the height of $0.8G_{max1}$, f_{11} and f_{12}, were measured (see Fig.3,curve c). And an iterative algorithm was used to separate the resonant peaks and possible shoulder peaks [54]. The three equivalent circuit parameter in the motional branch of primary resonator are calculated by:

$$R_1 = \frac{1}{G_{max1}} \qquad (6)$$

$$C_1 = \frac{(f_{12} - f_{11})G_{max1}}{\pi f_{10}^2} \qquad (7)$$

$$L_1 = \frac{R_1}{2\pi(f_{12} - f_{11})} \qquad (8)$$

Then the values of G_1 at the measuring frequencies were calculated by Eq.(4), and were deducted from the total conductivity-frequency curve. The residual conductance-frequency curve was used to estimate the equivalent circuit parameters of resonator 2 ($L_2C_2R_2$ branch). This process was continued until the equivalent circuit parameters of all the resonators were estimated. In the following iterative cycles, the equivalent circuit parameters were used as the initial values to deduct the conductance of other peaks from the total conductivity-frequency spectrum. The parameters of the target resonant peak were calculated again until stable values were obtained.

Fig.6 illustrates the changes in the resonant frequencies of the eight peaks during the stimulant convection process. With increasing convection time, the frequencies of the peaks were increased at a similar rate. But the peak with higher start frequency has shorter duration, expect the shoulder peaks. Obviously, the increase in the resonant frequencies the peaks was due to the decrease in surface mass loading on the QCM. Hence, it is possible to monitor the mass change by QCM even in the case of peak cleavage.
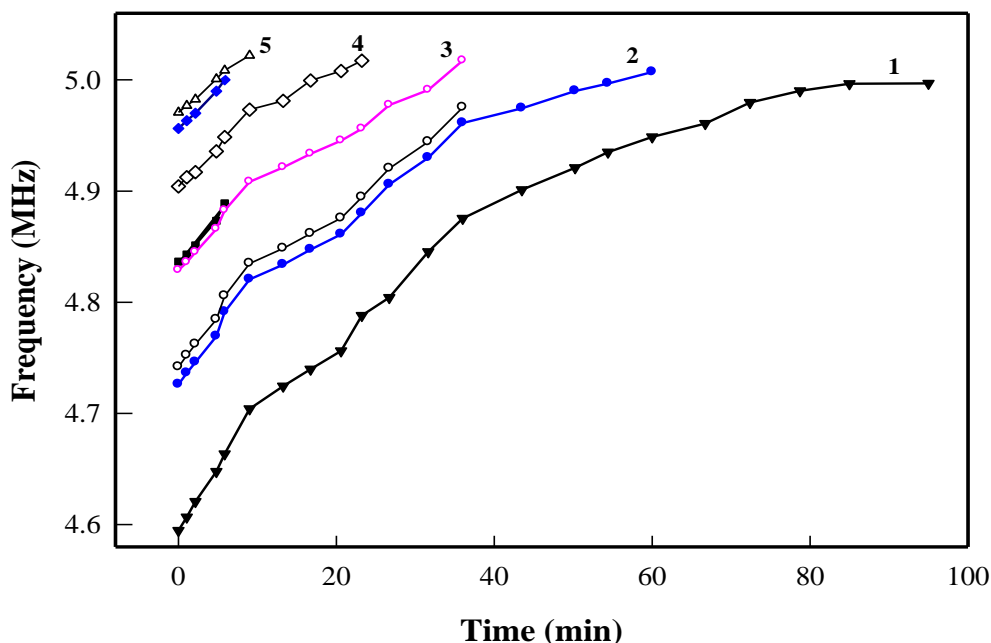
Figure 6. Frequency change of resonant peaks during the simulant convection process. The numerals corresponds to the resonant peaks in Fig.4A. The experimental conditions are the same as Fig.4.

In this work, the averaged resonant frequency with the square of the peak height, $\overline{F}_0$, is calculated by

$$\overline{F}_0 = \frac{\sum G^2_{\max i} f_{i0}}{\sum G^2_{\max i}} \tag{9}$$

where f_{i0} and $G_{\max i}$ are the resonant frequency and height of the *ith* peak, respectively. The weighting factor of $G^2_{\max i}$ emphasizes the contribution of the stronger resonant peak to $\overline{F}_0$.

Fig.7 shows the changes of $\overline{F}_0$ and the area of hoarfrost film (A_{ice}) on the electrode surface of QCM during the stimulant convection process. With the increasing convection time, the value of A_{ice} was decreased, the value of $\overline{F}_0$ was increased due to the decrease in mass loading. With the value of F_0 of the blank QCM as the reference, the follow regressed relation was obtained:

$$\Delta \overline{F}_0 \text{ (kHz)} = \overline{F}_0 - F_0 = -6.83 - 443.8 A_{ice} \text{ (cm}^2\text{)} \qquad (r^2 = .976) \tag{10}$$

Surely, the irregular ice film on QCM does not meet the prerequisite of uniformity in Sauerbrey equation. But the nearly-linear relation between $\Delta \overline{F}_0$ and A_{ice} suggests that $\overline{F}_0$ may be applicable to monitor the mass change of the ice film. As an attempt, the shifts in $\overline{F}_0$ were using to estimate the averaged mass of the ice film by Sauerbrey equation. For example, the averaged mass loading of 2.68 mg/cm^2 was calculated from the value of $\Delta \overline{F}_0$ for the initial ice film, corresponding to a thickness of 29.2 μm. With increasing convection time, the averaged mass loading of the ice film decreased linearly with increasing $\Delta \overline{F}_0$. This result exhibits the applicability of the $\overline{F}_0$ in the case of peak cleavage.
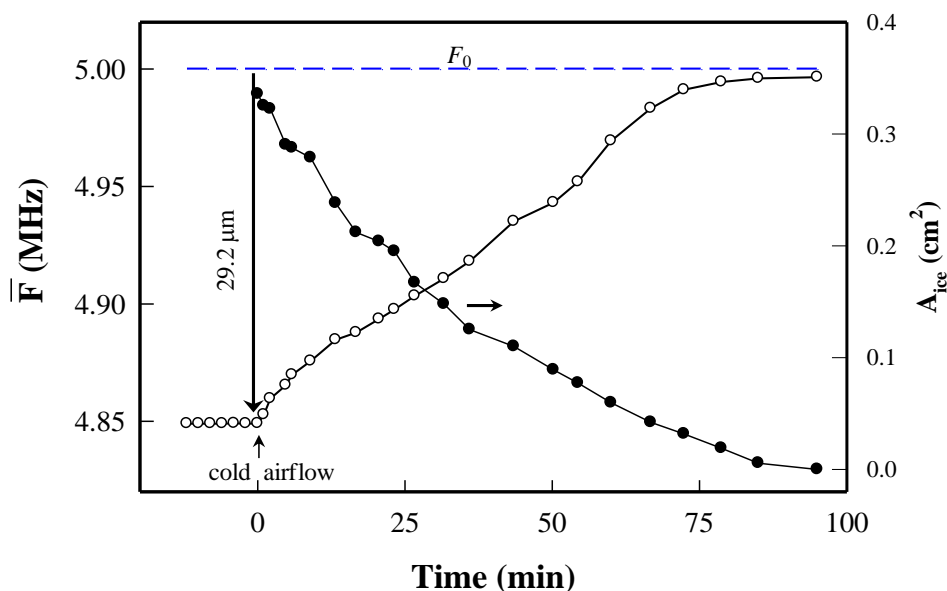
Figure 7. Change in averaged resonant frequency of QCM and residual area of ice film on the electrode surface during the simulant convection process. The experimental conditions are the same as Fig.4.

3.4 Monitor the interaction of ice film and ethanol vapor by QCM

In this experiment, the strategy of condensation water film on the surface of the QCM was employed to prepare ice film. When the thermal equilibrium was reached, a homogeneous and thin ice film was deposited on both sides of the QCM, which was indicated by the response of QCM. Under the conditions used, a single symmetrical sharp resonant peak was observed. The motional resistance of the QCM with a rigid ice film is in the range of 30~50Ω. The thickness of the prepared ice film was dependent on the contact time to the moisture.

Fig. 8 shows simultaneously recorded F and R_q of QCM with ice film during the absorption process of ethanol vapor on the ice film. As shown in Fig.8A, the initial resonant frequency of the QCM with ice film is 4.9762 MHz, which corresponds to the ice film with the total thickness of 4.26 μm. When a small volume of 2 μl ethanol was added in the adsorption box, the decrease in F reveals the increase in mass loading due to the adsorption of ethanol vapor on the ice film. Under the experimental condition used, F was decreased 512 Hz in 5 min while the value of R_q was unchanged. In the last stage of adsorption, a slight increase in F at an averaged rate of 2.1 Hz/min was observed. In the second addition of 2 μl ethanol, the value of F decreased another 292 Hz in 4 min then increase at an averaged rate of 6.5 Hz/min. The value of R_q increased by 5.2 Ω in this process. In the third addition of 2μl ethanol, F decreased initially 151 Hz then increased at an average rate of 33.7 Hz/min. The increase in R_q is 18.2 Ω in this stage. The increase in F and R_q is more obvious in the forth addition of 2 μl ethanol. After 4 min, the frequency is even higher than that with initial ice film before ethanol addition. The increase in F and R_q reveals that part of ice film was dissolved during absorption the vapor of ethanol. Hence, it is comprehensible that the adsorption of adsorption of methanol, acetone

and formaldehyde on ice film was preformed at low concentration of adsorbate under much lower timperture [55].
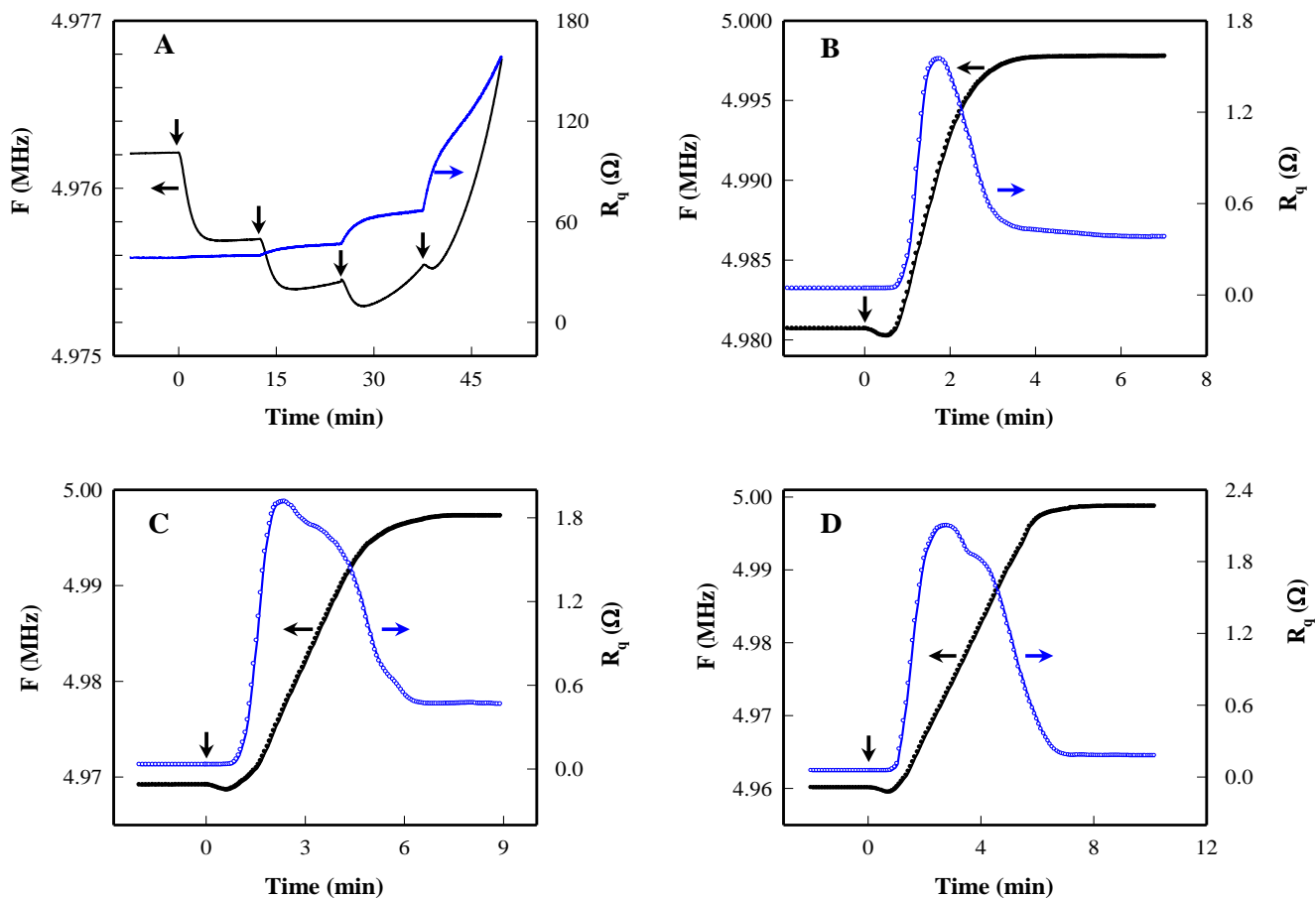

Figure 8. Change in resonant frequency and motional resistance of QCM with ice film during the absorption of ethanol vapor to ice   film. The adown arrows indicate the addition of ethanol into the absorption box. Amount of ethanol in an injection: (A) 2 µL; (B) 50 µL; (C) 50 µL; (D) 50 µL.

Fig.8B,C and D show the changes in F and R_q of the QCM with ice film during the absorption of ethanol of higher concentration. In this experiment, 50 µl ethanol was added in the absorption box. With the value of F_0 in the blank QCM as the reference, the initial frequency shifts in Fig.8 B,C and D are -19.56, -31.13 and -40.21 kHz, which corresponds to the total thickness of ice film of 3.46, 5.51 and 7.12 µm, respectively. It can be seen that F decreased to a minimum then increased rapidly until approached the stable values, which are less than the value of F_0 in the blank QCM. On the other hand, R_q increased sharply until a maximum then decreased to a plateau. As the thickness of ice film increased, the maximum of R_q increased.

Fig.9 illustrates the corrections of F and R_q of the QCM during the absorption process. Three types of F vs R_q were observed. Hence, the response of QCM was the combination of the mass and viscous effect. In the initial adsorption stage (a-b), F decreased while the R_q was nearly unchanged, the

mass effect due to the adsorption of ethanol on ice film is the main response model. In the middle absorption stage (b-c), both of F and R_q increased rapidly. This result indicates that the ice film was dissolved by the interaction of ice film and ethanol vapor. The transform of a rigid ice film to a liquid film resulted in the decrease in the mass loading, which was indicated by the increase in F. The increase in R_q is due to the dissolution of part of ice film, which increased in energy loss from the oscillating QCM surface.
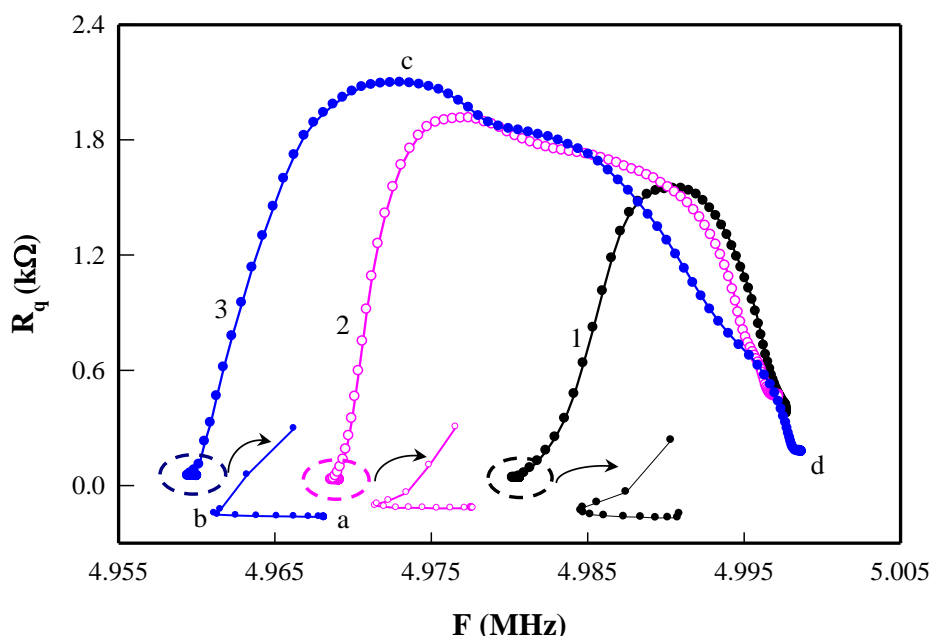

Figure 9. Correlation between the resonant frequency and motional resistance of QCM with ice film during the absorption process of ethanol vapor to ice film. Amount of ethanol added was 50 μL. Thickness of initial ice film: (1) 3.76μm; (2) 6.01μm; (3) 7.72 μm.

In contact mechanics and evaporation studies with the QCM, the influence of the contact area of a liquid drop on the response were investigated [56-60]. The dependence of frequency and bandwidth on film thickness and contact area is described within a sheet-contact model [61]. In the absorption process of ethanol vapor to ice film, the interfaces of electrode/liquid and ice/liquid were occurred on the surface of the QCM due to the dissolution of part of the ice film. Hence, the influence of the contact area on the response of QCM was added in the following equations.

$$\Delta F = -\frac{(A_1 + A_2)f_0^{3/2}}{A}[\frac{\eta\rho}{\pi\mu_q\rho_q}]^{1/2} \qquad (11)$$

$$\Delta R_q = \frac{(A_1 + A_2)(2\pi f_0\eta\rho)^{1/2}}{K^2} \qquad (12)$$

Where A_1 and A_2 are the contact area in the interfaces of electrode/liquid and ice/liquid, respectively.

With increasing the amount of ice film dissolved, the values of A_1 and A_2 increased, which resulted in the increase in R_q and an additional decrease in F. As shown in Fig.8, the maxima of R_q are 1569, 1912 and 2907 Ω for the QCM with initial ice film thickness of 3.46, 5.51 and 7.12 μm, respectively. In a control experimental, $R_q = 3302$ Ω was measured in 50% ethanol aqueous solution at

-18 °C. Although the concentration of ethanol in the liquid film was unknown, it is reasonable to consider that there is $A_1+A_2 < A$ even at the maximum of A_1+A_2. After separation the frequency shifts caused by the viscous effect by the slope of $\Delta F/\Delta R_q$= -2.157 Hz/Ω, the averaged thickness of the ice film can be estimated from the frequency shifts from the mass effect. Obviously, the mass effect has much more significantly impact on the frequency change of the QCM. It is shown that the maxima of R_q occurred at the points with 73.5%, 43.3% and 32.7% of ice film dissolved in the QCM with initial ice film thickness of 3.46, 5.51 and 7.12 μm, respectively.

In the shrinkage stage (c-d), the increase in F and decrease in R_q were observed. The decrease in R_q is due to the reduce in A_1+A_2. With increase in the amount of ice film dissolved, the value of A_2 was expected to decrease. It should be noted that the value of A_1 may be decreased by the shrinkage and volatilization of the liquid film. Because the liquid film is the mixture of water and ethanol, which has lower icing temperature and higher volatility than water. In fact, there was an ice film on the wall of the absorption box. After adding ethanol on the filter paper, the vapor of ethanol was preferentially absorbed by the ice film on QCM because the shorter diffusion distance. As the contact time increased, the concentration of ethanol vapor in the area near the QCM was reduced due to the diffusion and absorption by the ice film on the wall. Hence, part of the liquid film was volatilized by the action of concentration difference. As a result, the total contact area of the solid/liquid interface decreased. Thus, R_q decreased while F increased rapidly. If all of the ice film on the surface of electrode was dissolved (A_2=0), the response of QCM was due to the change in contact area of the liquid film. But the averaged values of $\Delta F/\Delta R_q$ in the late shrinkage stage are = -4.36, -5.32 and -7.75 Hz/Ω, in the samples with initial ice film thickness of 3.46, 5.51 and 7.12 μm, respectively. This result reveals that the frequency shifts are caused by both the mass and viscous even in the late shrinkage stage. As the residual liquid film on electrode surface was related to the variable surface tension, the stable value of F and R_q were different for each ice film. Under the conditions in Fig.8, the stable values are 4.9977, 4.9972 and 4.9987 MHz for the resonant frequency, 377, 461 and 173 Ω for motional resistance in QCM with the initial ice film thickness of 3.46, 5.51 and 7.12 μm, respectively. It can be seen that stable values of F are less than F_0 of the blank QCM and the value of R_q are larger obviously than that of QCM with the initial ice film. Hence, a small residual liquid film was expected to reserve on the electrode surface after the addition of ethanol in the adsorption box.

4. CONCLUSIONS

The results described above indicated that QCM technique is a useful tool to investigate the stability and adsorption behavior of ice film. It was shown that a freshly deposited ice film was lost at a considerable rate even at the temperature of -18 °C, especially for a thin ice film. Under our experimental condition, an ice film with thickness of 0.32 μm was disappeared by 96% in 1 min. The loss of the ice film may be due to the loose structure of the initial ice film. On the other hand, the response of QCM depends on the thickness and distribution of the surface mass loading. Normal symmetrical strong resonant peak is obtained in the case of a thin and homogeneous ice film. If a relative thick (ca. 29 μm) and asymmetrical ice film is formed on the electrode surface, the resonance

of the QCM is split to a group of small resonant peaks in a broad span of frequency. During a stimulant convection process, the thin ice film was disappeared gradually and irregularly, the resonant peaks moved to higher frequency with increasing intensity. The small peaks were merged gradually to one strong peak. The averaged resonant frequency of the peaks with the square of intensity as the weighting factor is in a near-linear correlation with the area of the ice film. The Sauerbrey equation may be applicable in the case with mulriple resonance. By the strategy to condense water film on the electrode surface, a homogeneous ice film is deposited. At the temperature of -18 °C, the ice film is dissolved partly or entirely after absorption of ethanol vapor. During the absorption process, the response of QCM with ice film is the combination of mass and viscous effect. For the QCM with an ice film of 7.12 μm, the averaged slopes of R_q vs F are -0.0013, 0.159 and -0.0894 Ω/Hz in the stages of initial adsorption, middle dissolution and late shrinkage and volatilization, respectively.

References

1. G. Sauerbrey, *Z. Phys.*, 155(1959)206.
2. N. Andreeva, T. Ishizaki, P. Baroch, N. Saito, *Sens. Actuators B,* 164 (2012) 15.
3. J. Xie, H. Wang, M Duan, *Sens. Actuators B*, 203 (2014) 239.
4. N. C. Speller,N. Siraj,B. P. Regmi,H. Marzoughi,C. Neal and Isiah M. Warner, *Anal. Chem.,* 87(2015)5156.
5. X. Jia, L. Tan, Q.J. Xie, Y.Y. Zhang, S.Z. Yao, *Sens. Actuators B*, 134 (2008) 273.
6. M. D. Levi, N. Levy, S. Sigalov, G. Salitra, D. Aurbach, J. Maier, *J. Am. Chem. Soc.*, 132 (2010)13220.
7. J. John, K. M. Hugar, J. Rivera-Meléndez, H. A. Kostalik, IV, Eric. D. Rus, H.S. Wang, G.W. Coates and H. D. Abruña, *J. Am. Chem. Soc.*, 136(2014)5309.
8. N. Shpigel, M. D. Levi, S. Sigalov, O. Girshevitz, D. Aurbach, L. Daikhin, N. Jäckel and V. Presser, *Angew.Chem. Int.Ed.*, 54(2015)12353.
9. G.N.M. Ferreira, A.C. da-Silva, B. Tomé, *Trends Biotechnol.*,27 (2009) 689.
10. C. I. Cheng, Y.P. Chang and Y.H. Chu, *Chem. Soc. Rev.*, 41(2012)1947.
11. Q.J. Liu, C.S. Wu, H. Cai, N. Hu, J. Zhou and P. Wang, *Chem. Rev.*,114(2014)6423.
12. Y.Q. Luo, T. Liu, J.M. Zhu, L.Y. Kong, W. Wang and L.Tan, *Anal. Chem.*,87(2015)11277.
13. F. Ma,A. Rehman,H. Liu,J.T. Zhang,S.L. Zhuand X.Q. Zeng, *Anal. Chem.*, 87(2015)1560.
14. Y.P. Zhou and Q.J. Xie, *Sens. Actuators B*, 223 (2016) 9.
15. B. Liu, M. Tu and R. A. Fischer, *Angew. Chem. Int. Ed.*, 52(2013)3402.
16. L.S. Liu, J.M. Kim and W.S. Kim, *Anal. Chem.*, 87(2015)3329.
17. Q.J. Xie, J. Wang, A.H. Zhou, Y.Y. Zhang, H.W. Liu, Z.N. Xu, Y. Yuan, M.Y. Deng, S.Z. Yao, *Anal. Chem.*, 71 (1999) 4649
18. I. Reviakine, D. Johannsmann and R. P. Richter, *Anal. Chem.*,83(2011) 8838.
19. Z.Q. Zhang, J.Y. Ye, P. Sun, Y. Yuan, Y.H. Tong, J.M. Hu, Y.H. Shao, *Anal. Chem.*, 74 (2002)1530.
20. S. N. Wren, D. J. Donaldson, *J. Phys. Chem. Lett.*, 2 (2011) 1967.
21. A. Chaulk, G. A. Stern, D. Armstrong, D. G. Barber, F.Wang, *Environ. Sci. Technol.*, 45(2011)1866.

22. S. N. Wren , D. J. Donaldson, *J. Phys. Chem. C*, 116 (2012)1017.
23. P. Pirzadeh, P. G. Kusalik, *J. Am. Chem. Soc.*, 135(2013)7278.
24. H. Watanabe, T. Otsuka, M. Harada, T Okada, *J. Phys. Chem. C*, 118 (2014)15723.
25. H.M. Wei,Y.Wei, X.Y. Lin, P. Liu, S.S. Fanand K.L. Jiang, Nano Lett., 15(2015)1843.
26. T. P. Liyana-Arachchi, K. T. Valsaraj, F. R. Hung, *J. Phys. Chem. A*, 116(2012) 2519.
27. S. Haq, J. Harnett, A. Hodgso, *J. Phys. Chem. B*, 106 (2002) 3950.
28. Ó. Gálvez, B. Maté, V. J. Herrero, R.Escribano, *Icarus*, 197 (2008) 599.
29. J. T. Newberg and H. Bluhm, Phys. Chem. Chem. Phys., 17(2015) 23554.
30. M. H. Kuo, S. G. Moussa and V. F. McNeill, J. Phys. Chem. C,118(2014)29108.
31. B. Collignon, S. Picaud, *Chem.Phys. Letts*, 393 (2004) 457.
32. T. P. Liyana-Arachchi, K. T. Valsaraj, F. R. Hung, *J. Phys. Chem. A*,115 (2011)9226.
33. S Picaud, P Jedlovszky, *Chem. Phys. Lett.* ,600 (2014)73.
34. Y. Tasaki ,T. Okada, *J. Phys. Chem. C*, 112 (2008) 2618.
35. M. Muro, M. Harada, T. Hasegawa, T. Okada, *J. Phys. Chem. C* , 116(2012)13296.
36. T. Bartels-Rausch, T. Huthwelker, H. W. Ga1ggeler, M. Ammann, *J. Phys. Chem. A*, 109 (2005)4531.
37. P. Behr, A. Terziyski, and R. Zellner, *J. Phys. Chem. A*, 110 (2006) 8098.
38. P. Parent, J. Lasne, G. Marcotte and C. Laffon, *Phys. Chem. Chem. Phys.*,13(2011)7142.
39. P. Ayotte, P. Marchand, J. L. Daschbach, R. S. Smith, B. D. Kay, *J. Phys. Chem. A*, 115 (2011)6002.
40. E. Park, D. H. Lee, S. Kimand H. Kang, *J. Phys. Chem. C*, 116(2012) 21828.
41. A.Symington, L.M.Leow, P.T. Griffiths, R. A.Cox, *J. Phys. Chem. A*, 116(2012)5990.
42. M. Szőri and P. Jedlovszky, *J. Phys. Chem. C*,118(2014)3599.
43. I.Sumi,S. Picaud and P. Jedlovszky, *J. Phys. Chem. C*, 119(2015)17243.
44. B.L. Mason, J.G. Dash, , *J. Geophys. Res.*, 105 (2000) 10185.
45. C. Delval, M. J. Rossi,*Phys.Chem.Chem.Phys.*, 6 (2004) 4665.
46. C. Delval, M. J. Rossi, *J. Phys. Chem. A*, 109 (2005) 7151.
47. A. Wucher, S.X. Sun, C. Szakal, N. Winograd, *Anal. Chem.*, 76 (2004)7234.
48. C. Szakal, J. Kozole, N. Winograd, *Appl. Surf. Sci.*, 252 (2006) 6526.
49. K.K. Kanazawa, J.G. Gordon, *Anal. Chim. Acta*, 117 (1985) 99.
50. H. Muramatsu, E. Tamiya, I. Karube, *Anal. Chem.*, 60 (1988) 2142.
51. P. Lörfgren, P. Ahlstöm, D.V. Chakarov, J. Lausmaa and B. Kasemo, *Surf. Sci.*,367 (1996) L19.
52. V.Tsionsky, L. Daikhin, D. Zagidulin, M. Urbakh and E. Gileadi, J. Phys. Chem. B,107 (2003) 12485.
53. A. Kaverin, V. Tsionsky, D. Zagidulin, L. Daikhin, E. Alengoz and E. Gileadi, J. Phys. Chem. B 108(2004) 8759.
54. L. Meng, X.C. Zhao, R. Sheng, P. Zhang, Q. Kang, D.Z. Shen, *Sens. Actuators B*, 147 (2010) 566.
55. A. K. Winkler, N. S. Holmes and J. N. Crowley, Phys. Chem. Chem. Phys., 2002, 4(2002) 5270.
56. C. M. Flanigan, M. Desai, K. R. Shull, *Langmuir*, 16 (2000)9825
57. M. J. Joyce, P. Todaro, R. Penfold,S. N. Port, J. A. W. May, C. Barnes, A. J. Peyton, *Langmuir*, 6(2000)4024.
58. N. T. Pham, G. McHale, M. I. Newton,B. J. Carroll, S. M. Rowan, *Langmuir*, 20(2004)841.
59. F. N. Nunalee , K. R. Shull, *Langmuir*, 20(2004)7083.
60. H. Zhuang,P. Lu, S. P. Lim, H. P. Lee, *Langmuir*, 23(2007)7392.
61. M. Kunze, K. R. Shull, D. Johannsmann, *Langmuir*, 22(2006)169.